Electron energy-dependent product state distributions in the dissociative recombination of O_2^+

Annemieke Petrignani[a)]
FOM Institute for Atomic and Molecular Physics, Kruislaan 407, 1098 SJ, Amsterdam, The Netherlands

Fredrik Hellberg, Richard D. Thomas, and Mats Larsson
Molecular Physics, Stockholm University, AlbaNova University Centre, SE-106 91 Stockholm, Sweden

Philip C. Cosby
Molecular Physics Laboratory, SRI International, Menlo Park, California 94025

Wim J. van der Zande
Institute for Molecules and Materials, Radboud University Nijmegen, Toernooiveld 1, 6525 ED Nijmegen, The Netherlands

(Received 14 March 2005; accepted 27 April 2005; published online 21 June 2005)

We present product state distributions and quantum yields from the dissociative recombination reaction of O_2^+ in its electronic and vibrational ground states as a function of electron collision energy between 0 and 300 meV. The experiments have been performed in the heavy-ion storage ring, CRYRING, and use a cold hollow-cathode discharge source for the production of cold molecular oxygen ions. The branching fractions over the different dissociation limits show distinct oscillations while the resulting product quantum yields are largely independent of electron collision energy above 40 meV. The branching results are well reproduced assuming an isotropic dissociation process, in contrast with recent theoretical predictions. © *2005 American Institute of Physics*. [DOI: 10.1063/1.1937388]

I. INTRODUCTION

Dissociative recombination (DR) of O_2^+ is one of the important reactions behind the green and red airglow in the Earth's atmosphere. It is even believed to be the only reaction responsible for the green airglow in the night time F region of the ionosphere. The $O(^1S)$ and $O(^1D)$ product atoms of the DR reaction radiatively relax to the $O(^1D)$ and $O(^3P)$ states giving rise to the green and red airglow, respectively. The exothermicity of the DR reaction for ground-state oxygen ions and zero-eV electrons can be as large as 7 eV. The resulting hot atoms have a distinct effect on atmospheric heating, on gravitational escape on, e.g., Mars and Venus, and on the terrestrial geocorona.[1,2]

The F region of the ionosphere where the DR of O_2^+ is mainly responsible for the red and green aurora is at roughly 150–250-km altitude. Here, the pressure is below 10^{-5} mbar, decreasing upon altitude, and the temperature is between 700 and 1000 K. The electron and the O_2^+ densities are on the order of 10^5 and 10^4 cm^{-3}, respectively, whereas the density of neutral species is orders of magnitude higher at 10^8 cm^{-3}. The O_2^+ ions can be rather efficiently quenched by their neutral counterparts giving rise to confusion as to the role of vibrationally excited O_2^+ in the production of $O(^1S)$.[3–5] The most probable collision energy between the electrons and the O_2^+ ions in the DR reaction, based on Maxwellian velocity distributions, is around 60 meV at 700 K and 85 meV at 1000 K. The mean free path of the product atoms can increase considerably at the low ionospheric pressure. The $O(^1S)$ product atoms, having a radiative lifetime of 0.71 s, as well as the $O(^1D)$ product atoms, with a radiative lifetime of 108 s, are able to relax radiatively. *In situ* atmospheric studies on the DR reaction of O_2^+ measure the green and/or the red airglow at 557.7 and 630.0 nm, respectively. These studies indicate that the vibrational excitation of the O_2^+ ions might be higher than expected, with the amount of excitation increasing upon altitude.[3,6,7]

In order to interpret and quantify the green and red airglow observations and their ionospheric implications, the dependence of the DR reaction on the O_2^+ internal excitation and the electron collision energy must be known. It has already been well established, both theoretically and experimentally, that the temperature dependence of the O_2^+ thermal rate coefficient follows the power law $\alpha(O_2^+) \sim T^{-0.7}$ or, in terms of electron-energy dependence of the rate coefficient as used in merged-beam experiments,[8–12] $k(O_2^+) \sim E_c^{-0.5}$. Here T pertains mainly to the electron temperature, while E_c is the collision energy between the electron and the ion. The dependence of the DR dynamics on either the vibrational excitation of the O_2^+ ions or on the electron collision energy is not well understood. Recently we reported a storage-ring experiment treating the vibrational dependence of the O_2^+ DR process, where we presented vibrationally resolved rate coefficients and branching fractions for the first time.[12] The earlier work of our group established the branching fractions for collision energies between 0 and 36 meV for O_2^+ ions in their electronic and vibrational ground states.[7] In this earlier paper, the theoretical prediction on the electron-energy dependence of the $O(^1S)$ quantum yield is also included.

a)Electronic mail: annemieke@petrignani.nl

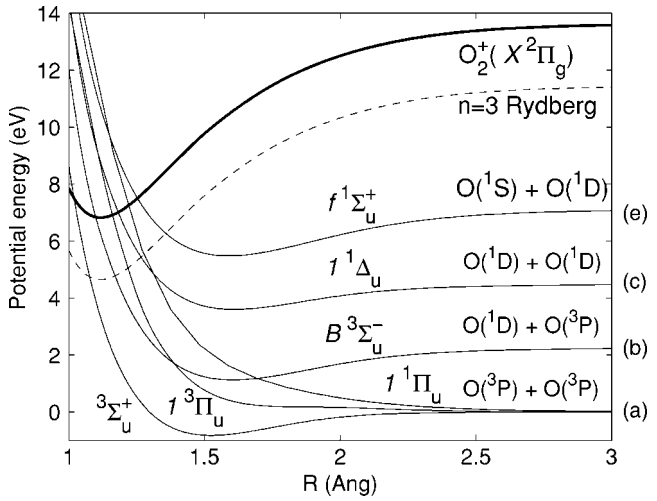

FIG. 1. Schematic of the diabatic potential curves relevant for the DR of O_2^+. The dissociation limits connected with each valence capture state are given on the right. The labels (a)–(c), and (e) refer to Eqs. (1a)–(1c) and (1e), respectively.

The possible DR reaction pathways for ground-state ions are shown in Eqs. (1a)–(1e). There are five dissociation limits energetically possible with kinetic-energy releases (KERs) varying from 0.8 to 6.95 eV for zero-eV electrons. The next dissociation limit is not reached until an additional 1.41 eV of energy is introduced, either vibrationally or through E_c.

$$O_2^+(X\,^2\Pi_g, v=0) + e^-(E_c)$$

$$\rightarrow O(^3P) + O(^3P) + (6.95 + E_c)\ \text{eV}, \quad (1a)$$

$$\rightarrow O(^1D) + O(^3P) + (4.99 + E_c)\ \text{eV}, \quad (1b)$$

$$\rightarrow O(^1D) + O(^1D) + (3.02 + E_c)\ \text{eV}, \quad (1c)$$

$$\rightarrow O(^1S) + O(^3P) + (2.77 + E_c)\ \text{eV}, \quad (1d)$$

$$\rightarrow O(^1S) + O(^1D) + (0.80 + E_c)\ \text{eV}. \quad (1e)$$

Figure 1 shows a number of potential-energy curves relevant for the process under study. The diabatic, doubly excited, repulsive, valence state curves cross the ionic state near the equilibrium separation of the ion, ensuring a finite Franck–Condon overlap. Moreover, all the valence states shown have a significant electron capture matrix element as evaluated by Guberman.[13] Note that most dissociation limits are associated with only a single dominating diabatic state.

In the present paper, we have extended the electron-energy-dependence study to the energy region of 0–300 meV using electronic and vibrational ground-state O_2^+ ions in order to determine the temperature-dependent branching relevant to atmospheric modeling (up to 1000 K). The results are presented as branching fractions as well as quantum yields and are discussed within the context of theoretical considerations. Attention is also given to the angular dependence of the DR reaction.

II. EXPERIMENT

The experiments were performed at the heavy-ion storage ring, CRYRING, at the Manne Siegbahn Laboratory (MSL) in Stockholm. The electron-energy dependence of the DR process has been studied through the product distributions using an imaging technique at 13 different collision energies chosen between 0 and 300 meV. Using this imaging technique, we can determine the KERs in the DR process [see Eqs. (1a)–(1e)]. The O_2^+ ions were formed in a water-cooled hollow-cathode ion source (JIMIS), a high-pressure source known to produce vibrationally cold ions. The extracted ions were then magnetically mass/charge selected and preaccelerated to 40 keV before injection into the storage ring whereafter the ion beam was further accelerated to 2.9 MeV. This acceleration takes 1.1 s to complete. The storage ring has a circumference of 51.6 m. It consists of 12 straight sections of which one is the interaction region, called the electron cooler. Here a cold electron beam is merged with the ion beam over a distance of 0.80 m. The detection system is located in a zero-degree arm following the electron cooler at a distance of 6.3 m from the center of the cooler. During storage the ions pass the electron cooler many times and the translational temperature of the ions is reduced by interaction with the cold electron beam. By changing the energy of the electron beam, the relative velocity and therefore the collision energy is varied. At 0-eV collision energy, the electron velocity is matched to the ion velocity. Due to the high MeV beam energies, the electron collision energy can be tuned accurately over a large dynamic range. In practice, the collision energy resolution in the CRYRING near 0 eV is approximately 2 meV. This is the limit given by the transverse velocity spread. The resolution worsens at elevated collision energies, and at 200 meV it is about 5 meV.[14] Additionally, the DR signal rate decreases quickly upon increasing collision energy; longer data acquisition times at higher collision energies were therefore used to compensate for the loss in signal rate.

The DR reactions take place in the electron cooler. For each event, the two neutral product O atoms, unaffected by the bending magnet after the cooler, will fly along a straight line into the zero-degree arm to the imaging setup. They hit a stack of microchannel plates followed by a phosphor screen. Light from the phosphor screen is imaged onto an image intensifier, which is used as an amplifier and a fast switch. Its output is focused onto a charge-coupled device (CCD) camera system and the fragment positions are recorded on an event-by-event basis.

Detailed descriptions of the detection system can be found elsewhere.[15] Collision-induced dissociation and charge-transfer reactions between the ions and the rest gas in the ring take place throughout the ring. This process limits the lifetime of the ion beam.[11] The charge-transfer reactions also give rise to two neutral fragments and form a background contribution in the DR measurement. This background is measured with the electron beam turned off or with the collision energy turned up high, where no or negligible DR signal is present, respectively. The acquired spectra in the present study are two-dimensional (2D) projections of

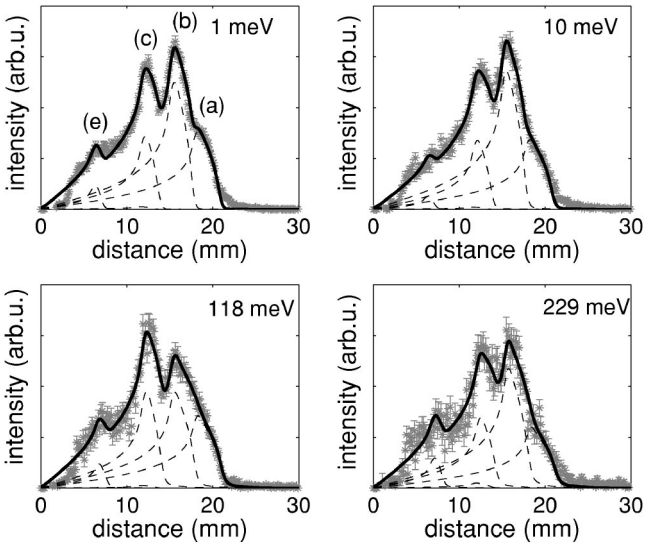

FIG. 2. The distance distributions of the DR of O_2^+ at collision energies of 1, 10, 118, and 229 meV (space-charge corrected energies). The stars are the experimental data and the solid curves are the simulations based on isotropic distributions. The peaks corresponding to the dissociation limits given in Eqs. (1a)–(1c) and (1e) are indicated at 1 meV with the labels (a)–(c) and (e), respectively. The dashed lines show the contributions of the dissociation limits as results from the fits.

the separations between the dissociating atoms. The difference in the arrival time of the two O atoms in each reaction is on the order of nanosecond and difficult to measure.[11,16] The effects of the 2D projection along with the length of the electron cooler are taken into account in the model for the distance distributions, which is extensively described elsewhere.[17,18] The toroidal region, i.e., the region where the electron beam merges into and demerges out of the ion beam, provides a collision region in which the electron collision energy is much larger than in the remainder of the electron cooler.[15] This toroidal effect is corrected for,[19,20] as is the electron space-charge effect, which affects the electron energy due to the presence of positive ions trapped in the space charge of the electron beam.[21]

III. RESULTS AND ANALYSIS

The dissociation dynamics were studied at 13 different values of the collision energy. A selection of the acquired spectra is shown in Fig. 2. These spectra show the distance distributions at collision energies of 1, 10, 118, and 229 meV (space-charge corrected energies). The measured data (stars) show a clear difference in branching behavior for the different energies. At $E_c = 10$ meV the $O(^1S) + O(^1D)$ dissociation limit [peak (e)] is hardly visible. Previous research[11] showed a disappearance of the $O(^1S)$ peak at 11 meV. Figure 2 also shows the fits corresponding to the different spectra (solid curves). They are determined by a weighted least-squares optimization procedure for each E_c separately, while using isotropic model projections[17] for all five dissociation limits [see Eqs. (1a)–(1e)] and only their branching fractions as free parameters. The model used includes a rotational temperature of the molecular ions of 300 K and assumes only $v=0$ parent ions; however, a small contribution of $O_2^+(X\,^2\Pi_g, v=1)$ ions cannot be fully excluded from the fits. The demagnification factor of the optical system between the phosphor and the CCD camera is optimized once for all spectra. The discrepancy between the fit and the measured data near 0-mm separation is due to the inability of the data acquisition software to distinguish between two close/overlapping hits on the detector. At low collision energies, a weak signal is observed at distances above 22 mm, pointing at higher KER values that cannot be fitted using $v=0$ ions only nor using any other low vibrational level. The discrepancy between the fit and the data decreases upon increasing collision energy. Above 100 meV the fitted models can describe the entire measured spectrum.

The derived branching fractions for all investigated collision energies are listed in Table I. The $O(^1S) + O(^3P)$ channel [see Eq. (1d)] is not listed; it was included in all the fits but turned out not to contribute to the acquired spectra with an uncertainty of about 1%. Its absence is predicted by quantum-chemical models and can also be inferred from other experimental information.[11,12,17,22–24] All branching fractions are shown in Fig. 3. The corresponding errors have been estimated from repeating the optimization using a large number of synthetic spectra modified with a Monte Carlo procedure in accord with their statistical error. The errors do not take into account the possibility of systematic errors due to, for example, inhomogeneities of the detection system, the possible presence of anisotropy in the DR reaction, or some contamination of vibrationally excited ions. As a reference, the reduced cross section, which is the DR cross section multiplied by the collision energy, is also presented.[12] The

TABLE I. The branching fractions and quantum yields for the different investigated collision energies. The $O(^1S) + O(^3P)$ channel [Eq. (1d)] is not listed due to its insignificant contribution.

E_c (meV)	1	10	45	78	101	118	142	176	188	211	229	235	281
$O(^3P)+O(^3P)$ [Eq. (1a)]	32[a]	29	24	29	33	32	31	25	22	28	27	26	29
$O(^1D)+O(^3P)$ [Eq. (1b)]	43	49	52	37	33	35	39	45	54	48	45	47	41
$O(^1D)+O(^1D)$ [Eq. (1c)]	20	20	20	29	27	28	26	23	19	17	22	21	24
$O(^1S)+O(^1D)$ [Eq. (1e)]	4	2	4	4	6	5	4	6	5	5	6	5	5
$O(^3PP)$	1.07[b]	1.06	0.99	0.94	0.98	0.97	1.00	0.93	0.96	1.03	0.97	0.97	0.97
$O(^1D)$	0.88	0.90	0.95	1.00	0.94	0.97	0.95	0.98	0.97	0.89	0.94	0.95	0.96
$O(^1S)$	0.04	0.02	0.04	0.04	0.06	0.05	0.04	0.06	0.05	0.05	0.06	0.05	0.05

[a]The branching fractions are rounded to the nearest integer value and may not add up to 100% due to rounding errors and the exclusion of the $O(^1S) + O(^3P)$ channel.

[b]The quantum yields may not add up to two-due to the exclusion of the $O(^1S) + O(^3P)$ channel.

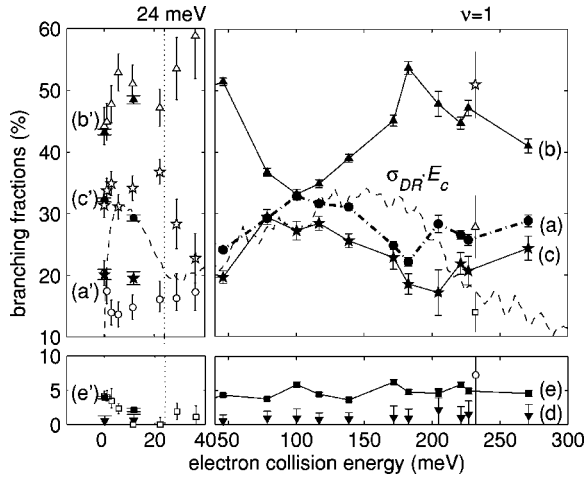

FIG. 3. The branching fractions for the different dissociation limits at all investigated collision energies. The figure is cut into four bordering and differently scaled regions. The left two regions show the present (filled symbols) and previous (unfilled symbols) (Ref. 11) branching fractions for $E_c=0-40$ meV as well as the energy position of the fine-structure splitting of the $O_2^+(X\,^2\Pi_g, v=0)$ at 24 meV. The right two regions show the present results for $E_c>40$ meV (filled symbols) and the branching fractions of $O_2^+(v=1)$ at the energy position of 232 meV (unfilled symbols) (see Ref. 12). The dissociation limits are as follows: $O(^3P)+O(^3P)$ (●), $O(^1D)+O(^3P)$ (△), $O(^1D)+O(^1D)$ (⋆), $O(^1S)+O(^3P)$ (▽), and $O(^1S)+O(^1D)$ (□). For clarity the limits are additionally labeled (a)–(e) and (a′)–(e′) for the present and previous (Ref. 11) branching fractions, respectively, corresponding to Eqs. (1a)–(1e). In the top two regions the reduced cross section (arbitrarily scaled in intensity), $\sigma_{DR}\cdot E_c$ is also included (dashed curve) (see Ref. 12). This line indicates at what energies resonances in the cross section occur. The fine-structure splitting as well as the vibrational energy spacing proceed a cross-section resonance minimum. See text for the description of the results.

DR cross section due to the direct DR process decreases inversely proportional to the collision energy. Hence the product of cross section and collision energy is constant in the absence of any other process than the direct DR mechanism. The coarse structure that can be observed in Fig. 3 is indicative of resonant processes such as in the indirect DR mechanism, in which capture initially takes place into molecular Rydberg states. The reduced cross section shows minima near 30 and 250 meV, which may also be accompanied by changes in branching behavior.

The observed branching behavior shows the following aspects. Branching to the $O(^1S)+O(^1D)$ limit [label (e)] starts at about 4% at 0 eV and goes down to 2% at 10 meV. Earlier research, which focused on the branching in the 0–40-meV region, shows a continuous decrease in the $O(^1S)$ yield down to zero between 0 and 11 meV, and a finite $O(^1S)$ yield up to 40 meV.[11] Above 40 meV, our results indicate that the $O(^1S)$ yield remains around a constant of 5%. Small, but significant oscillations can be observed that do not seem to be correlated with structures in the reduced cross section, nor clearly with the branching behavior to the other limits. We do not observe any value that is significantly larger than 5% nor do we observe a strong increase with electron collision energy. As will be discussed later (see Sec. IV), the latter could have been expected. The branching to $O(^3P)+O(^3P)$ [label (a)] and $O(^1D)+O(^1D)$ [label (c)] behaves in an approximately similar fashion. Their absolute values are about the same but, more importantly, they show similar variations as a function of collision energy above 40 meV. Below 40 meV, they differ significantly. The behavior above 40 meV could be suggestive of a single capture channel, which during the dissociation process distributes itself over these two dissociation limits. Below $E_c=40$ meV, the relative importance of the $O(^3P)+O(^3P)$ limit is higher than the $O(^1D)+O(^1D)$ limit. For all energies, the most dominant dissociation limit is the mixed $O(^1D)+O(^3P)$ limit [label (b)] with values up to 50%. In view of the fact that the total branching sums up to unity, the minimum in the dominant channel occurs at the energy where the two other channels show a maximum. The $O(^1S)+O(^3P)$ channel [label (d)] is found to be consistently smaller than 2% and insignificantly present, an explicit experimental verification of the absence of this channel in the DR process. Figure 3 also shows the energy of the fine-structure splitting of the $O_2^+(X\,^2\Pi_g, v=0)$ level at 24 meV as well as the ~232 meV, which have been determined in a recent study in our group on the vibrational dependence of the DR branching.[12] Both characteristic energies precede a resonance minimum in the DR cross section. The vibrational energy has a completely different effect from that of electron collision energy on the DR dynamics. More specifically, the $O(^1S)+O(^1D)$ contribution of 14% for $v=1$ is much higher than the ~5% at 229-meV collision energy.

Earlier research in our group reported branching fractions for electron collision energies up to 36 meV in small energy increments (see Fig. 3).[7,11] The present $O(^1S)+O(^1D)$ [label (e)] and the $O(^1D)+O(^3P)$ [label (b)] dissociation limits agree well with these previous results. The $O(^1S)$ production drops significantly in both cases at an energy around 11–12 meV, whereas the $O(^1D)+O(^3P)$ goes up. However, the present branching fractions to the $O(^3P)+O(^3P)$ [label (a)] and $O(^1D)+O(^1D)$ [label (c)] limits, at the two investigated energies in this region, are significantly different from the previous measurements. The dissociation limits are more or less reversed. This reversal in branching fractions to the $O(^3P)+O(^3P)$ and the $O(^1D)+O(^1D)$ limit will give rise to a change in the $O(^1D)$ and $O(^3P)$ quantum yields.

Figure 4 shows the quantum yields. The quantum yield is the number of atoms produced in a specific state for an average DR event. Hence, the quantum yields sum up to two in the case of the DR of O_2^+. The values of the quantum yields are listed in Table I. As can be observed in Fig. 4, the $O(^1D)$ and $O(^3P)$ quantum yields are relatively insensitive to the collision energy and surprisingly similar. For practical purposes the $O(^1D)$ and $O(^3P)$ quantum yields could be assumed to have averages of 0.95 ± 0.04 and 0.99 ± 0.04, respectively, independent of collision energy. This nearly energy-independent behavior is an intriguing result in view of the significant variations observed in the branching fractions. The $O(^3P)$ quantum yield is generally larger than the $O(^1D)$ quantum yield. At the investigated collision energy of 79 meV the quantum yields of $O(^1D)$ and $O(^3P)$ are nearly equal. This corresponds to the drop in branching towards the mixed $O(^1D)+O(^3P)$ dissociation limit and precedes the similar behavior of the two dissociation limits $O(^3P)+O(^3P)$ and $O(^1D)+O(^1D)$ (see Fig. 3). For reference pur-

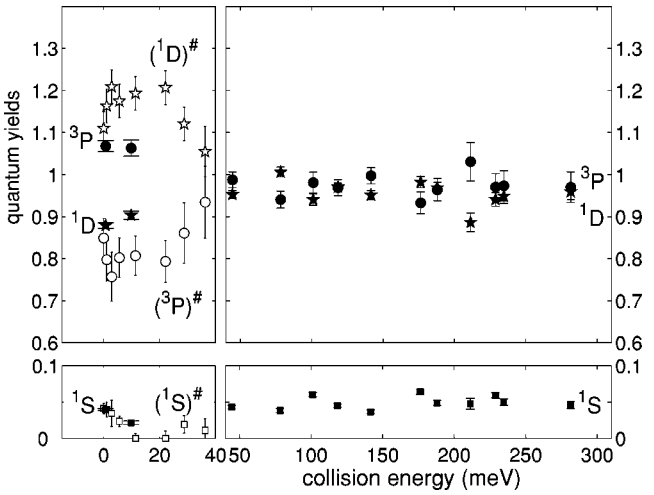

FIG. 4. The quantum yields at the investigated collision energies [excluding the $O(^3P)+O(^1S)$ channel]. The figure is cut into four differently scaled regions. Note that the scale in the quantum yield jumps from 0.1 for the lower to 0.6 for the upper regions. The left two regions show the present (filled symbols) and previous (unfilled symbols) (Ref. 11) quantum yields for $E_c=0-40$ meV. The right two regions show the present results for $E_c>40$ meV (filled symbols). The quantum yields are as follows: $O(^3P)$ (●), $O(^1D)$ (⋆), and $O(^1S)$ (□). For clarity the yields are additionally labeled according to their excited state (the symbol # refers to the previously determined yields). See text for the description of the results.

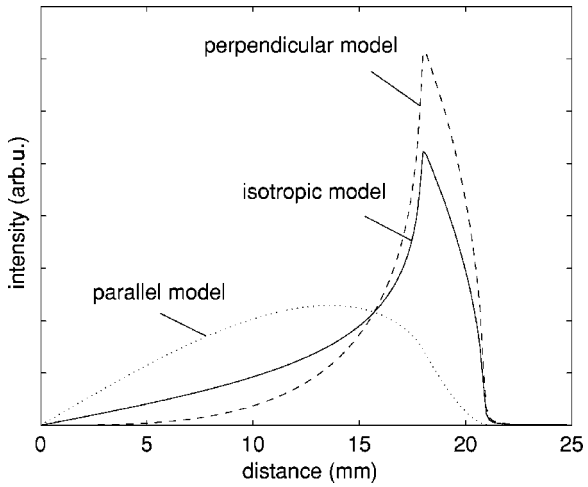

FIG. 5. The shape of the 2D model distance distributions for a single dissociation limit as used to fit the imaging data from a storage-ring experiment; in the case of isotropic (solid curve), preferably perpendicular (dashed curve), and preferably parallel (dotted curve) dissociations. The perpendicular and parallel preferences are described in terms of $\cos^2\theta$ and $\sin^2\theta$, where θ is the angle between the orientation of the dissociation and the beam axis. The shown model distributions include a KER of 6.95 eV, a 300-K rotational temperature, a finite interaction region length of 85 cm, and the toroidal correction.

poses the quantum yields from our earlier collision energy-dependence research are shown.[11] The observed differences are directly related to the difference we observe in the branching. Finally, the $O(^1S)$ quantum yield equals the branching fraction of $O(^1S)+O(^1D)$. The small oscillations that can be observed do not seem to be correlated with the patterns in the quantum yields of $O(^1D)$ and $O(^3P)$ atoms.

A. Anisotropy

Isotropic distributions have been assumed for all dissociation limits and investigated collision energies; this means that all relative orientations of the low-energy electron and the molecular axis are assumed to have equal DR cross section. However, possible anisotropies in the DR reaction can affect the shape of the 2D distance distributions. In fact, the efficiency of collision reactions between electrons and molecular ions often depends on the relative orientation of the incoming electron and the molecular axis for reasons of symmetry. As it is believed that the DR reaction is very fast on a rotational time scale, a preferred axis orientation will show up in the distance distribution. In our experiment, the relative velocity at nonzero collision energies is perpendicular to the detector plane. The model distance distributions corresponding to a single channel dissociating isotropically, with a perpendicular preference, and with a parallel preference are shown in Fig. 5. The preferences to perpendicular and parallel dissociations are described in terms of $\cos^2\theta$ and $\sin^2\theta$, respectively, where θ is the angle between the orientation of the dissociation and the beam axis. A strong preference for the ion to dissociate parallel to the relative velocity gives a distribution that is much less peaked at the maximum possible distance than in the case of a strong preference for the molecular orientation perpendicular to the relative velocity, which is parallel to the detector plane in our experiment. It has recently been reported that distributions in DR processes may be more complex.[25] These distributions, $I(\theta)$, may not be correctly described with only one parameter as in $I(\theta)\propto 1+\beta P_2(\cos\theta)$, where β is the so-called anisotropy parameter and $P_2(\cos\theta)$ is the second-order Legendre polynomial. Higher-order Legendre polynomials may be necessary. Complex distributions may result when DR reactions at low collision energy are dominated by a single partial wave, $l\lambda$, with $l>1$ and $\lambda>0$. It is noted that in principle each dissociation channel may have a different anisotropy when a dissociation limit is connected to a specific molecular symmetry of the initial capture state.

We investigated the possibility of anisotropy in the present observed distributions at all investigated energies. The nominal 0-eV distribution is included as well, although no preferred relative velocity is present at 0-eV collisions. However, it is sometimes argued that an intrinsically present anisotropy in the merged-beam experiment can still be detected because of the anisotropy of the velocity distribution of the electrons in the reaction region; the velocity spread parallel to the ion-beam velocity is smaller than the velocity spread perpendicular. To the best of our knowledge, no anisotropy has ever been observed at 0 eV. It has been observed for higher energies, such as in the DR of NO^+, where a perpendicular preference was found for one of the dissociation channels at 1-eV collision energy.[15,26]

Figure 6 shows the fits for the present distributions at $E_c=1$-, 10-, 118-, and 229-meV collision energies based on predicted angular distributions for the different dissociation limits in the DR of O_2^+.[25] This prediction states that the $O(^3P)+O(^3P)$ ground-state limit is related to a preference towards parallel dissociation and the other four limits are related to a preference towards perpendicular dissociation. All fits result in roughly 70% dissociating into the ground-

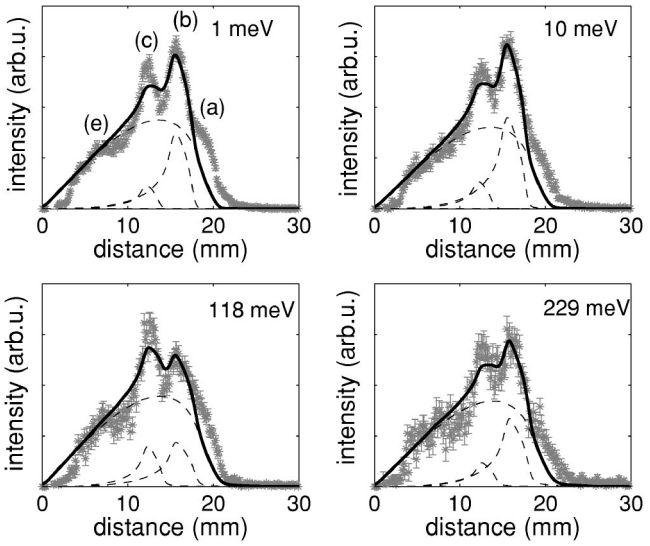

FIG. 6. The distance distribution of the DR of O_2^+ at 1, 10, 118, and 229 meV (space-charge corrected energies). The stars are the experimental data and the solid lines are the fits based on the angular distributions predicted by Guberman. The peaks, (a)–(c), and (e), correspond to the dissociation limits given in Eqs. (1a)–(1c) and (1e), respectively. The dashed lines show the contributions of the dissociation limits as results from the fits, where the $O(^1S)$ contribution [peak (e)] is zero.

state limit. As can be observed, the large $O(^3P)+O(^3P)$ contributions arise from the two features of the perpendicular distribution. There is no clear peak present and the maximum that is observed occurs at much lower distances. As a consequence, the observed shoulder at large particle separation and the structure observed for the remaining channels cannot be reproduced properly, in spite of the fact that the perpendicular distribution is more sharply peaked. The isotropic distributions give the best fit for all dissociation channels at all investigated collision energies between 0 and 300 meV. Additionally, the $O(^3P)$, $O(^1D)$, and $O(^1S)$ quantum yields as derived from the anisotropic fits at all energies are above 1.5, under 0.5, and 0, respectively. We can add two arguments against the use of these quantum yields apart from the experimental observation that the fits using isotropic distributions result in better fits. First, the $O(^1D)$ quantum yield has been determined to be closer to unity, which is in agreement with the present isotropic fit. Previous determinations include laboratory experiments other than storage-ring experiments[27,28] and *in situ*[29–32] measurements where values between roughly 0.8 and 1.5 are found at the altitude regions where the DR of ground-state O_2^+ mainly determines the $O(^1D)$ production. Second, the experiment near 0-eV collision energy is expected to yield close to isotropic distributions. Using anisotropic distributions for higher collision energies causes drastic changes in the derived branching fractions and quantum yields that are not easily understood.

IV. DISCUSSION

The branching behavior in the DR of ground-state O_2^+ ions has been studied with a merged-beam technique at collision energies between 0 and 300 meV. The present experiment has covered the energy gap between the ground and first excited vibrational levels of O_2^+ (232 meV). Over this relatively small energy window the branching fractions depend strongly on the collision energy. The branching oscillates as a function of energy for the three dominant channels. The distance between the observed minima is about 150 meV, smaller than the vibrational spacing in the parent ion state (see Fig. 3). Dissociation towards the $O(^1S)+O(^1D)$ limit behaves differently. The branching starts at a value of about 5% at 0 eV and then drops to 2% around 10 meV, which is consistent with the previous observation, where the $O(^1S)+O(^1D)$ branching was found to disappear between 11 and 22 meV. Above 40 meV, the present branching remains between 4% and 6% with small, but significant variations. The $O(^1D)$ and $O(^3P)$ quantum yields have only weak sensitivity to the collision energy and changes stay within 5%, quite similar to the small percentile changes (10%) in the results of Peverall *et al.*[11] Average values of 0.99 ± 0.04 and 0.95 ± 0.04 for the $O(^3P)$ and $O(^1D)$ yields, respectively, may be used in practice. Interestingly, the quantum yields as predicted by a model involving only statistical branching arguments and spin-conservation rules are 1.06, 0.82, and 0.12 for $O(^3P)$, $O(^1D)$, and $O(^1S)$, respectively.[33]

According to Guberman,[25] six diabatic channels provide effective routes for the DR of the lower vibrational levels of O_2^+ (see Fig. 1): $^3\Pi_u(^3P+^3P)$, $^1\Pi_u(^3P+^3P)$, $A\,^3\Sigma_u^+(^3P+^3P)$, $B\,^3\Sigma_u^-(^1D+^3P)$, $f\,^1\Sigma_u^+(^1S+^1D)$, and $^1\Delta_u(^1D+^1D)$. The dissociation limit corresponding to each capture state is given between the parentheses, i.e., the limits that are linked to the capture states when the Rydberg-valence interactions do not affect the dissociation behavior. Apart from the ground-state dissociation limit, the three excited limits are served by only one symmetry, allowing for the predictions on the expected anisotropy.[25] A number of other electronic states, such as the $O_2^*(^{1,3}\Pi_g)$, have favorable crossings but unfavorably small electron capture matrix elements.[34] These states are disregarded as relevant because of the small associated electron capture widths. The reason for mentioning them here is the fact that, for example, the diabatic $O_2^*(^1\Pi_g)$ valence state has a crossing with an excited $O_2^*(^1\Pi_g)$ valence state resulting in a distribution of flux over the $O(^3P)+O(^3P)$ and $O(^1D)+O(^1D)$ dissociation limits, such as is seen in the present results. The dominance of the mixed $O(^1D)+O(^3P)$ limit points to the importance of the $^3\Sigma_u^-$ state in the DR process, although this limit is also the dominant channel for the $O_2^*(^3\Pi_g)$ valence state. Another reason for mentioning states other than the six states nominally taken into account is the apparent contradiction between the predicted anisotropy of the fragments and the observed distance distributions. Although heavy-ion storage-ring 2D experiments do not have sufficient resolving power for precise angular distributions, dissociations with the molecular axis parallel to the collision velocity will show up clearly as nonisotropic.[15]

The lack of agreement between our observed isotropy and the predicted angular dependencies[25] deserves further attention. These theoretical predictions agree with the rules derived by Dunn[35] for electron-impact processes and with the predictions of O'Malley and Taylor[36] for dissociative attachment. Dissociative attachment has distinct similarities with DR, but it lacks the long-range Coulomb attraction between the electron and the target. However, the predicted

angular dependencies additionally involve both a selection of the active valence states in the process, based on the magnitudes of the Franck–Condon overlap and electron capture matrix element, as well as the identification of the active electron partial waves in the process at our low electron energies. The treatment of the anisotropy further assumes that the DR process is sudden on the time scale of molecular rotation. This aspect is generally assumed to be correct for DR, as the reaction competes with autoionization, which is a very fast process (fs).

In an early paper by Guberman,[37] a mechanism was proposed that explained the production of a quantum yield of $O(^1S)$ atoms of a few percent in the DR of O_2^+ at small energies. In this mechanism, spin-orbit coupling between Rydberg states of $^3\Sigma_u^-$ and $^1\Sigma_u^+$ characters results in flux to the $O(^1S)+O(^1D)$ limit. The initial electron capture takes place into the $^3\Sigma_u^-$ state while forming a Rydberg state of the same symmetry resonantly near zero energy. The vibrational excited character of this Rydberg state takes care of a sufficient elongation of the molecular bond such that the Franck–Condon overlap with the $f\,^1\Sigma_u^+$ allows dissociation towards an $O(^1S)$ atom. The rapid decrease in the $O(^1S)$ quantum yield observed below 20-meV collision energy provides strong support of this *resonant* mechanism.[7] The relevance of the small $O(^1S)+O(^1D)$ channel should not be underestimated. Before invoking this spin-orbit mechanism, $O(^1S)$ quantum yields of much less than 0.01 were expected. If direct access of the repulsive $f\,^1\Sigma_u^+$ becomes possible, a strong increase in the branching fraction could be expected to result from the exponential increase in the overlap between the vibrational wave functions in the initial and final electronic states. Indirect processes can also have significant influence on the final branching when varying the collision energy. The spin-orbit coupling and indirect processes have been included in Guberman's calculation of the $O(^1S)$ quantum yield and show many resonances with varying collision energies, especially above 100 meV (see Fig. 2 in Ref. 7). The mechanism cannot explain the observed weakly oscillating branching above 40 meV. The present $O(^1S)$ quantum yields are much more constant, even after accounting for the decrease in resolution with increasing collision energy, which smoothes the resonant structure of Guberman's prediction.

The results reported here agree with our previous results from measurements at 0 eV in a vibrationally hot ion beam.[12] The branching fractions and quantum yields do not entirely agree with earlier measurements from our group that were taken at energies between 0 and 40 meV in a cold ion beam,[11] nor with the measurements performed at ASTRID by Kella *et al.* (at 0 eV).[17] The latter experiment, however, involved the vibrationally excited mixed-isotope $^{16}O^{18}O^+$ and a single determination using vibrationally independent branching behavior. Both vibrational-dependent branching and isotope effects may contribute.[12,38] Our earlier experiment at 0–40 meV differs from the present setup as it involved a more complicated data acquisition method in order to record arrival-time differences of the product atoms. A multiline photomultiplier was set to select two-particle events only, requiring accurate settings of all trigger levels. In all position-sensitive detection techniques, detector inhomogeneities may affect the results. Fortunately in storage-ring experiments, the fragment distances are not much larger than the distribution of center-of-mass positions, which is a measure for the O_2^+ beam size at the position of the detector. The large beam size reduces the effects of detector inhomogeneities. On the other hand, a large beam size may have a discriminating effect on large KER events; the associated large fragment distances may more easily result in one of the fragments falling outside the detection area. For the DR of O_2^+ this would especially affect the $O(^3P)+O(^3P)$ channel [see Eq. (1a)], resulting in an underestimation of the $O(^3P)$ and subsequently in a too large $O(^1D)$ quantum yield. We investigated the beam size and found no indication of missing events. Additionally, we simulated a DR experiment at 0 eV using the present branching fractions and then assumed a too large beam size to investigate its effect. This simulation shows that our branching fractions in combination with a discriminating effect due to a large beam size can give rise to distance distributions as observed in Ref. 11. It seems possible that discrimination of the large KER events contributed to the earlier measurements. There is no reason known to us to explain the reverse situation, i.e., where the $O(^3P)+O(^3P)$ branching fraction would be overestimated instead of underestimated. Although the current results have been reproduced in two independent experimental runs, the presence of an unidentified systematic effect cannot be ruled out. Since the variations in the collision energy are very small with respect to the KER values, each systematic effect will impact all the results in a similar way.

V. CONCLUSIONS

The present measurements of O_2^+ DR products are made over a sufficiently wide range of electron collision energies to allow temperature-dependent quantum yields and branching fractions to be defined at electron temperatures below 1000 K. We observe smooth and distinct oscillations in the branching fractions. Resonant behavior does not seem to appear in the dissociative behavior. The resulting quantum yields are largely independent of the collision energy. Moreover, we find that the distributions at all investigated energies can be described with isotropic distributions. In spite of the apparent simplicity of the DR reaction, it is clear that progress still has to be made in both experiment and theory before we arrive at a complete picture.

ACKNOWLEDGMENTS

This work is part of the research program of the "Stichting voor Fundamenteel Onderzoek der Materie (FOM)," which is financially supported by the "Nederlandse Organisatie voor Wetenschappelijk Onderzoek (NWO)." It has been partially supported by the EU research-training network Electron Transfer Reactions (ETR) under Grant No. HPRN-CT-2000-00142. We thank the staff of the Manne Siegbahn Laboratory for their part in making the experiments possible and we thank Steven Guberman for valuable discussions.

[1] J. L. Fox, J. Geophys. Res. **102**, 24005 (1997).
[2] R. R. Hodges, Jr., J. Geophys. Res. **105**, 6971 (2000).
[3] D. R. Bates and E. C. Zipf, Planet. Space Sci. **28**, 1081 (1980).
[4] E. C. Zipf, J. Geophys. Res. **85**, 4232 (1980).
[5] M. R. Torr and D. G. Torr, Rev. Geophys. Space Phys. **20**, 91 (1982).
[6] D. R. Bates, Planet. Space Sci. **40**, 893 (1992).
[7] R. Peverall, S. Rosén, M. Larsson *et al.*, Geophys. Res. Lett. **27**, 481 (2000).
[8] F. L. Walls and G. H. Dunn, J. Geophys. Res. **79**, 1911 (1974).
[9] J. W. McGowan, P. M. Mul, V. S. D'Angelo, J. B. A. Mitchell, P. Defrance, and H. R. Froelich, Phys. Rev. Lett. **42**, 373 (1979).
[10] P. M. Mul and J. W. McGowan, J. Phys. B **12**, 1591 (1979).
[11] R. Peverall, S. Rosén, J. R. Peterson *et al.*, J. Chem. Phys. **114**, 6679 (2001).
[12] A. Petrignani, W. J. van der Zande, P. C. Cosby, F. Hellberg, R. D. Thomas, and M. Larsson, J. Chem. Phys. **122**, 014302 (2005).
[13] S. L. Guberman, in *Dissociative Recombination: Theory, Experiment and Applications I*, edited by J. B. A. Mitchell and S. L. Guberman (World Scientific, Singapore, 1989), pp. 45–60.
[14] M. Larsson, Annu. Rev. Phys. Chem. **48**, 151 (1997).
[15] F. Hellberg, S. Rosén, R. Thomas, A. Neau, M. Larsson, A. Petrignani, and W. J. van der Zande, J. Chem. Phys. **118**, 6250 (2003).
[16] S. Datz, R. Thomas, S. Rosén, M. Larsson, A. M. Derkatch, F. Hellberg, and W. J. van der Zande, Phys. Rev. Lett. **85**, 5555 (2000).
[17] D. Kella, L. Vejby-Christensen, P. J. Johnson, H. B. Pedersen, and L. H. Andersen, Science **276**, 1530 (1997); Science **277**, 167(E) (1997).
[18] W. J. van der Zande, J. Semaniak, V. Zengin *et al.*, Phys. Rev. A **54**, 5010 (1996).
[19] M. B. Någård, J. B. C. Pettersson, A. M. Derkatch *et al.*, J. Chem. Phys. **117**, 5264 (2002).
[20] A. Neau, A. Al Khalili, S. Rosén *et al.*, J. Chem. Phys. **113**, 1762 (2000).
[21] A. Al-Khalili, S. Rosén, H. Danared *et al.*, Phys. Rev. A **68**, 042702 (2003).
[22] H. Helm, I. Havell, C. W. Walter, and P. C. Cosby, in *Dissociative Recombination: Theory, Experiment and Applications III*, edited by D. Zajfman, J. B. A. Mitchell, D. Schwalm, and B. R. Rowe (World Scientific, Singapore, 1996), pp. 139–150.
[23] S. L. Guberman, J. Chem. Phys. **67**, 1125 (1977).
[24] S. L. Guberman, Int. J. Quantum Chem. **S13**, 531 (1979).
[25] S. L. Guberman, J. Chem. Phys. **120**, 9509 (2004).
[26] L. Vejby-Christensen, D. Kella, H. D. Pedersen, and L. H. Andersen, Phys. Rev. A **57**, 3627 (1998).
[27] J. L. Queffelec, B. R. Rowe, F. Vallée, J. C. Gomet, and M. Morlais, J. Chem. Phys. **91**, 5335 (1989).
[28] E. C. Zipf, Bull. Am. Phys. Soc. **15**, 418 (1970).
[29] J. Semeter, M. Mendillo, J. Baumgardner, J. Holt, D. E. Hunton, and V. Eccles, J. Geophys. Res. **101**, 19683 (1996).
[30] J. H. A. Sobral, H. Takahashi, M. A. Abdu, P. Muralikrishna, Y. Sahai, and C. J. Zamlutti, Planet. Space Sci. **40**, 607 (1992).
[31] H. Takahashi, B. R. Clemsha, P. P. Batista, Y. Sahai, M. A. Abdu, and P. Muralikrishna, Planet. Space Sci. **38**, 547 (1990).
[32] V. J. Abreu, S. C. Solomon, W. E. Sharp, and P. B. Hays, J. Geophys. Res. **88**, 4140 (1983).
[33] W. J. van der Zande, in *Dissociative Recombination: Theory, Experiment and Applications IV*, edited by M. Larsson, J. B. A. Mitchell, and I. F. Schneider (World Scientific, Singapore, 2000), pp. 251–260.
[34] S. L. Guberman, in *Physics of Ion-Ion and Electron-Ion Collisions*, edited by F. Brouillard and J. W. McGowan (Plenum, New York, 1983), pp. 167–200.
[35] G. H. Dunn, Phys. Rev. Lett. **8**, 62 (1962).
[36] T. F. O'Malley and H. S. Taylor, Phys. Rev. **176**, 207 (1968).
[37] S. L. Guberman, Science **278**, 1276 (1997).
[38] S. L. Guberman, in *Dissociative Recombination: Theory, Experiment and Applications IV*, edited by M. Larsson, J. B. A. Mitchell, and I. F. Schneider (World Scientific, Singapore, 2000), pp. 111–120.